coatings

MDPI

Article

Development of Nickel Electrodes for Molten Carbonate Fuel Cells: Performance Characterization and Optimization of the Manufacturing Process

Martino Prati [1], Dario Bove [1,*], Roberto Spotorno [2] and Barbara Bosio [1]

[1] Department of Civil, Chemical and Environmental Engineering (DICCA), University of Genoa, Via Opera Pia 15, 16145 Genoa, Italy; martino.prati@edu.unige.it (M.P.); barbara.bosio@unige.it (B.B.)
[2] Department of Chemistry and Industrial Chemistry, University of Genoa, Via Dodecaneso 31, 16146 Genoa, Italy; roberto.spotorno@unige.it
* Correspondence: dario.bove@unige.it

Abstract

The growing need to reduce CO_2 emissions and promote the energy transition has driven the development of high-efficiency electrochemical technologies such as Molten Carbonate Fuel Cells (MCFCs), which can simultaneously generate electricity and capture CO_2. This work focuses on the development of nickel electrodes produced by electrodeposition, a technique that enables precise control over the morphology and porosity of the deposited material. The experimental activity mainly investigated the influence of electrical parameters (current density and potential difference) and deposition time on metal film growth, with the aim of optimizing the porous structure and enhancing electrochemical performance. The prepared samples were characterized in terms of mass, thickness, and morphology by scanning electron microscopy, confirming consistency with Faraday's law. Subsequently, the electrodes were tested in cell stations to evaluate their electrochemical behavior under operating conditions representative of MCFC operation. The results demonstrated that an appropriate combination of electrical parameters and deposition time enables the formation of uniform, porous nickel coatings suitable for electrolyte retention. Electrodeposition thus proved to be an effective and scalable approach for the fabrication of optimized nickel electrodes for molten carbonate fuel cell applications.

Keywords: molten carbonate fuel cells; nickel electrodes; electrodeposition; porous structure

Academic Editor: Je Moon Yun

Received: 29 December 2025
Revised: 5 February 2026
Accepted: 9 February 2026
Published: 12 February 2026

1. Introduction

Molten Carbonate Fuel Cells are distinguished by their dual functionality, which makes them one of the most promising technologies in the field of sustainable energy conversion [1,2]. On the one hand, they enable the generation of electrical power without direct combustion, thus reducing pollutant emissions and achieving higher efficiency compared to conventional systems [1]. On the other hand, due to the transport of carbonate ions (CO_3^{2-}) through the electrolyte, MCFCs are capable of capturing CO_2 during operation [3]. Such a feature makes them particularly attractive in the context of the energy transition and the decarbonization of industrial processes, especially in hard-to-abate sectors such as steel and cement production, heavy transport and petrochemicals [4–6]. In the maritime sector, recent studies have investigated retrofit-oriented CO_2 mitigation solutions to comply with IMO (International Maritime Organization) targets, analyzing both innovative shipboard

CCS systems based on thermally and electrically heated steam methane reformers for removal rates ranging from 20% to 80%, and molten carbonate fuel cell-based configurations capable of achieving a 20%–40% CO_2 reduction while simultaneously producing additional power, with results showing that system performance strongly depends on engine specific fuel consumption, route length and retrofit constraints [4,6]. In the steel sector, the integration of molten carbonate fuel cells enables deep decarbonization of furnace exhaust gases, achieving CO_2 reductions exceeding 100% when fueled with biomethane and at least 85% even with fossil methane [6]. In cement plants, MCFC integration enables CO_2 capture from flue gases with high carbon dioxide concentration, while achieving net electric efficiencies of about 46% and exporting up to 35 MWe, fully covering plant auxiliary consumption and enabling clean power generation [5].

Within the cell, the electrodes play a crucial role in determining overall performance, as they directly influence the kinetics of the electrochemical reactions, the internal resistance, and the operational lifetime of the device. The electrodes are generally made of porous nickel-based materials, selected for their stability under both oxidizing and reducing conditions, as well as for their excellent electrical conductivity and mechanical strength. In particular, the anodes are typically composed of nickel alloys, such as nickel chromium or nickel aluminum, which provide improved corrosion resistance and structural stability under MCFC operating conditions [7]. The microstructural features, particularly the porosity and pore size distribution, vary depending on whether the electrode functions as an anode or a cathode, since they must promote the diffusion of reactant gases and the proper ionic transport at the electrode—electrolyte interface [8]. For the cathode, the target pore size ranges from 7 to 15 μm, with an overall porosity between 70% and 80%. In contrast, the anode is designed with smaller pores, typically between 3 and 6 μm, and a porosity of approximately 55% [7]. Traditionally, MCFC electrodes are fabricated through a tape casting process followed by high-temperature sintering. Although conventional fabrication methods based on powder processing and high-temperature sintering provide good electrochemical performance, they are associated with high energy consumption, due to sintering temperatures typically above 800–1000 °C, long processing times often extending over several hours or days, and limited flexibility in tailoring electrode microstructure and porosity [1]. To overcome these limitations, electrodeposition has been proposed as an alternative technique capable of operating at low temperatures while offering precise control over the morphology and porosity of the deposit through the adjustment of electrochemical parameters.

The goal is to obtain porous electrodes with morphological and structural characteristics comparable to those of conventional sintered electrodes, but through a more economical and sustainable process. For this purpose, nickel substrates were used onto which a superficial nickel layer was electrodeposited to reproduce the porosity and pore size typical of MCFC electrode materials [7]. The electrodepositions were carried out using a Watts bath, a standard electrolyte solution in nickel plating processes, characterized by a high initial concentration of Ni^{2+} ions [2,3]. The optimization of the deposition parameters and the subsequent morphological and functional characterization of the obtained electrodes aim to evaluate the effectiveness of this technique as a viable alternative to traditional manufacturing methods for Molten Carbonate Fuel Cell applications.

2. Materials and Methods

2.1. Substrates

Nickel felt substrates (Bekaert, Kortrijk, Belgium) were used as deposition substrates. The felts exhibited a fibrous structure with thicknesses ranging from 0.25 to 0.50 mm and an average porosity of approximately 66%, suitable for porous MCFC electrode applications [7].

Prior to electrodeposition, all samples were subjected to acid pickling in a 10% hydrochloric acid aqueous solution. Each specimen was immersed three times and then thoroughly rinsed with demineralized water to remove residual acid.

2.2. Watts Electrolytic Bath

The electrolytic bath employed in this study was the conventional Watts bath, a standard electrolyte for nickel electrodeposition, consisting of three main components: Nickel sulfate hexahydrate ($NiSO_4 \times 6H_2O$, purity $\geq$ 99.0%), nickel chloride hexahydrate ($NiCl_2 \times 6H_2O$, purity $\geq$ 98.0%), and boric acid (H_3BO_3, purity $\geq$ 99.5%) were employed as chemical reagents. All materials were supplied by Sigma-Aldrich (St. Louis, MO, USA) and used as received without further purification. The pH of the electrolytic bath was maintained within the range of 3.5–4.5 and periodically monitored using pH indicator paper. The quantities of the components were determined for the preparation of one liter of electrolyte solution. Deionized water was subsequently added to adjust the solution to the final volume. The quantities of the reagents are reported in Table 1 [8–10].

Table 1. Electrolyte composition for 1 L of Watts bath (molar concentrations).

Component	Concentration [M]
Nickel sulfate	1.14
Nickel chloride	0.25
Boric acid	0.65
Deionized water	To volume (1 L)

The electrolyte solution was prepared by gradually adding the components to promote uniform mixing and complete dissolution, thereby preventing the formation of agglomerates. The process was assisted by mild heating on a hot plate combined with magnetic stirring. An optimal temperature range of 30–50 °C was identified, ensuring sufficiently fast dissolution kinetics without causing thermal degradation of the bath components [11,12]. A pure nickel sheet was used as sacrificial anode, ensuring a stable nickel ion concentration in the electrolytic bath during the duration of the process.

2.3. Experimental Parameters

Electrodeposition was carried out under galvanostatic conditions, with constant applied current and variable cell potential [10,11]. The process was conducted using a DC power supply manufactured by Eutron (Rivoli, Italy). The anodic sheets were immersed to a depth corresponding to theoretical current densities of approximately 300 $A \cdot m^{-2}$ at the anode and 400 $A \cdot m^{-2}$ at the cathode. These values were purely indicative and were not adopted in the final experiments. Higher current densities were applied to achieve a significant increase in the deposited mass [11,12].

The felt samples were cut to dimensions of 4 cm $\times$ 3 cm with an active area of 3 cm $\times$ 3 cm exposed to the electrolyte for deposition, while the remaining portion was used for the electrical connection to the clamp. Pure nickel sheets with dimensions of 3.0 cm $\times$ 5.0 cm $\times$ 0.1 cm were used as sacrificial anodes. The temperature of the Watts bath was maintained at 45 $\pm$ 5 °C, ensuring adequate ionic conductivity and stable deposition conditions. The temperature was monitored using a digital infrared thermometer manufactured by Bosch (Gerlinger, Germany).

Oxidation tests were performed on electrodeposited nickel samples to determine the parabolic oxidation rate constant under high-temperature oxidizing conditions. To experimentally determine the parabolic oxidation rate constant of nickel, nickel felt samples were used, each cut to a standard size of 2 $\times$ 2 cm. Prior to the thermal treatment, all

samples were subjected to acid cleaning in a 10% HCl solution, followed by thorough rinsing with deionized water, in order to remove any impurities and contaminants present on the sample surface. The samples were then oxidized in a furnace under a constant air flow of 15 L/min for five different durations (2, 4, 8, 12, and 16 h), with five samples prepared for each time interval. The mass of each sample was measured before and after oxidation using an analytical balance (precision 0.0001 g). The mass change was subsequently normalized to the sample surface area. All samples were placed on a ceramic support resistant to high temperatures and subjected to the same thermal cycle: heating and cooling at 5 °C/min, with a holding step at 700 °C for the prescribed duration.

A further characterization was carried out to measure the skeletal density and void fraction of the nickel-plated felt samples, in order to obtain information on the substrate morphology and porosity. The skeletal density and void fraction of the nickel-plated felt samples were determined by water pycnometry. Bulk density was calculated from the sample mass and geometric volume. These quantities were measured for the nickel felt samples using an analytical balance and a Vernier caliper (Neoteck, Barbarano Mossano, Italy).

3. Results and Discussion

The results are presented combining qualitative morphological observations and quantitative analyses. SEM images are used to qualitatively illustrate the electrodeposition behavior, while gravimetric, structural, and electrochemical measurements provide the quantitative basis for the discussion. Based on the experimental results, nickel-based materials are confirmed as highly attractive for MCFC applications due to their excellent resistance to corrosion in oxidizing and high-temperature environments, good mechanical stability under load, and outstanding chemical compatibility with the molten carbonate electrolyte [1].

The first experimental step focused on evaluating the evolution of the electrodeposited layer as a function of the immersion time in the electrolyte bath. Keeping all electrical and thermal parameters constant, three electrodepositions were performed on nickel felt samples, with deposition times set to 5, 7.5, and 10 min. The experiments were carried out in galvanostatic mode, maintaining a constant current intensity of 3 A throughout each deposition. All nickel felt samples were prepared according to the dimensions described above, with a defined active area exposed to electrodeposition and an uncoated region reserved for clamp attachment. According to Faraday's law, and under fixed material and current density conditions, the mass of metal deposited varies linearly with the electrodeposition time. This linear dependence makes the immersion time a key parameter for controlling the thickness and morphology of the resulting deposit. Figure 1 shows a sequence of SEM images of the nickel felt samples electrodeposited for different immersion times. The same magnification is maintained to make the progressive growth of the deposit over time more evident. SEM observations clearly highlight a progressive growth of the nickel layer with increasing immersion time, resulting in improved coating continuity while preserving the intrinsic fibrous morphology of the nickel felt. This feature is particularly relevant for MCFC electrodes, where high porosity and an interconnected pore network are essential to ensure effective gas diffusion and electrolyte retention. Overall, these results indicate that electrodeposition represents a viable and flexible technique for the fabrication of porous nickel electrodes for MCFC applications.

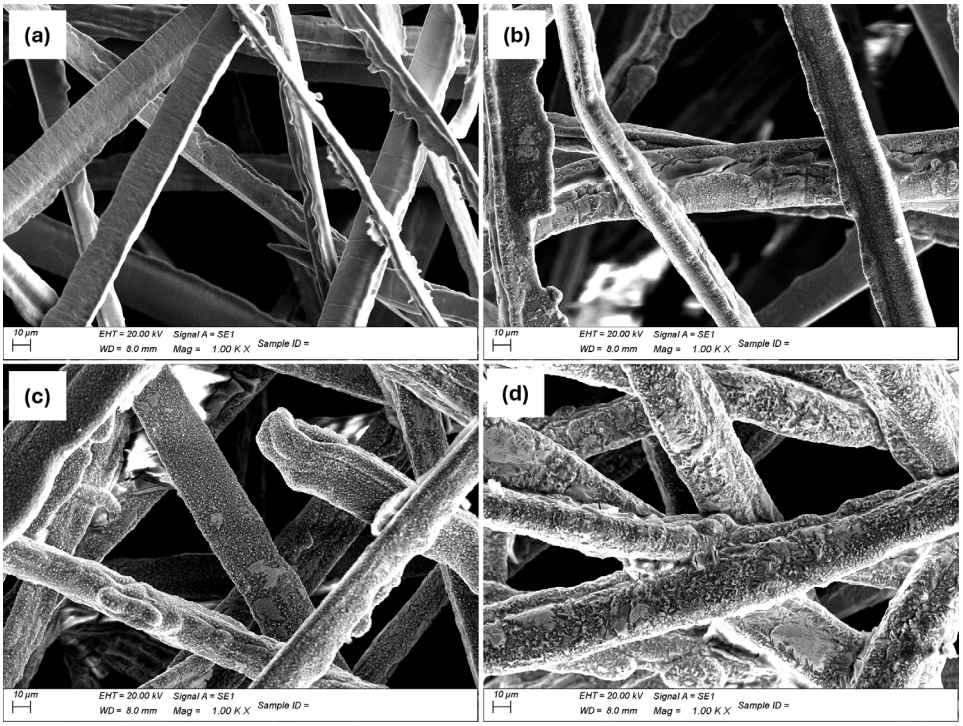

Figure 1. Sequence of SEM images showing the evolution of the morphology of the electrodeposited samples as a function of deposition time. (**a**) non-plated nickel felt; (**b**) felt after 5 min of electrodeposition; (**c**) felt after 7.5 min of electrodeposition; (**d**) felt after 10 min of electrodeposition.

An additional verification of Faraday's law was performed by selecting five different current-time pairs designed to yield the same theoretical deposited mass. Based on the ideal cathodic current density reported in Section 2.3, a reference condition of 360 mA applied for 30 min was first defined, and the corresponding theoretical nickel mass was calculated using Faraday's equation. The remaining current–time combinations were then determined by appropriately adjusting the applied current and deposition time in order to maintain a constant theoretical deposited mass. In this way, each experiment was expected to produce an identical amount of deposited material, ensuring full comparability among the samples and providing an internal validation of Faraday's law. Five nickel felt samples were therefore prepared and electrodeposited according to the selected current–time pairs. For each sample, the post-deposition mass variation was measured and compared with those of the other samples. A statistical analysis was also performed to assess the reliability and accuracy of the measurements. All tests were carried out in galvanostatic mode to allow precise control of the applied current. The deposition temperature was maintained at approximately 40 °C to ensure uniform operating conditions. Table 2 reports the selected time-current pairs and the corresponding mass variations in the samples. The experimental results showed a clear linear relationship between the deposited mass and the product of applied current and deposition time, confirming the reliability and predictability of the galvanostatic electrodeposition process when precise control of mass loading is required. This aspect is particularly important for MCFC electrodes, where even small deviations in active material loading may significantly affect electrochemical performance.

Table 2. Time-current pairs and the corresponding mass variation obtained.

Time [min]	Current Intensity [mA]	Mass Variation [g]
7.5	1440	0.207
15	720	0.225
30	360	0.226
45	270	0.251
60	180	0.261

To verify the reliability of the measurements, a statistical analysis was performed on the deposited mass data. Specifically, the standard deviation was calculated for each sample with respect to the theoretically predicted deposited mass. The resulting standard deviation values were then averaged and normalized to the mean deposited mass in order to determine the coefficient of variation, defined as the ratio between the standard deviation and the arithmetic mean. The obtained coefficient of variation is 9.27%, which is below the commonly accepted threshold of 10% and can therefore be considered consistent with the validity of Faraday's law [13]. The good agreement between theoretical and experimental values further confirms the reproducibility of the electrodeposition process under the investigated conditions and supports its suitability for the controlled fabrication of nickel-based porous electrodes.

3.1. Measurement of the Parabolic Rate Constant of Nickel

The increase in oxide thickness therefore follows a parabolic behavior, described by Equation (1) [14].

$$x^2 = k_p t \tag{1}$$

where x is the sample thickness $[m]$, k_p is the parabolic rate constant $\left[m^2 s^{-1}\right]$, and t is the time $[s]$. The parabolic rate constant quantifies the oxide growth rate.

Experimentally, k_p can be determined by measuring the mass gain of the sample exposed to an oxidizing atmosphere and normalizing it with respect to the surface area. By linearizing Equation (2), the value of the parabolic rate constant can be obtained as the slope of the resulting line, which is derived by plotting the surface mass change as a function of time Equation (2).

$$\left(\frac{\Delta m}{A}\right)^2 = k_p t \tag{2}$$

Maintaining identical operating conditions ensured the reproducibility of the measurements and the reliable determination of the parabolic rate constant. The obtained results are reported in Figures 2 and 3. High-temperature oxidation tests provided insight into the stability of nickel under conditions representative of MCFC operation. The experimentally observed oxidation behavior follows a parabolic trend, indicating that oxide growth is governed by diffusion-controlled ionic transport through the oxide scale, in agreement with well-established oxidation models for nickel at high temperatures [14–16].

The parabolic rate constant derived from the gravimetric measurements, on the order of 10^{-10} g^2 cm^{-4} s^{-1}, is consistent with values reported in the literature for nickel oxidation at comparable temperatures, confirming the validity of the experimental approach adopted in this study [14]. These results demonstrate the suitability of nickel for high-temperature operation in oxidizing environments and provide quantitative insight into its oxidation kinetics under conditions representative of MCFC operation.

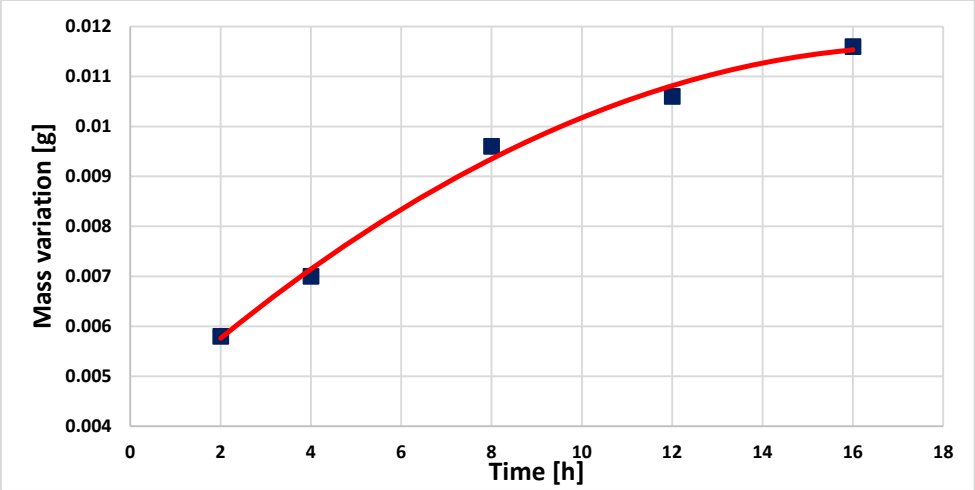

Figure 2. Parabolic trend of the mass variation as a function of oxidation time for nickel felt samples. The blue squares represent the experimentally obtained data points, corresponding to the mass variations of the samples as a function of time. The red curve represents the consistency of the data with the parabolic fit performed.

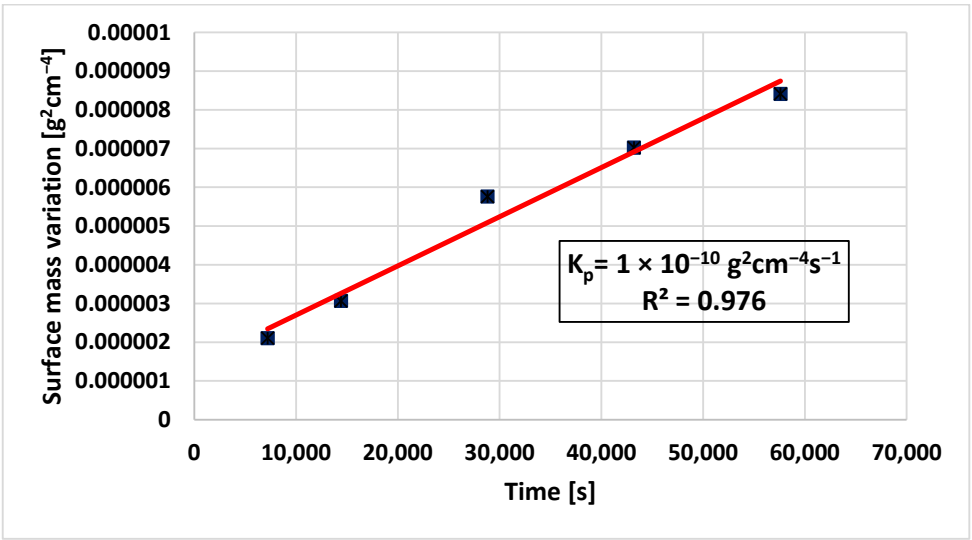

Figure 3. Linearization of the parabolic law used to extract the parabolic rate constant. The blue squares represent the experimentally obtained data points, corresponding to the squared mass change per unit area of the samples as a function of time. The red line represents the consistency of the data with the linear fit performed.

3.2. Measurement of Density and Void Fraction by Pycnometry

For each sample, the measured skeletal density values and the corresponding absolute standard deviation are reported as an indicator of the measurement reliability (Table 3). For the measurement of skeletal density and degree of porosity, the samples previously prepared for the verification of Faraday's law were used. To distinguish the different felt samples, each specimen was identified according to its immersion time in the Watts bath. Porosity is obtained from the ratio between the bulk density which includes the volume of the pores and the skeletal density measured by pycnometry, which corresponds only to the solid material Equation (3). Consequently, the bulk density must always be lower than the skeletal density.

Table 3. Skeletal density values obtained for the nickel felts, with the corresponding absolute standard deviations.

	Skeletal Density [g/cm^3]	Dev. Absolute Standard [g/cm^3]
Felt	3.561	0.33
Felt 7.5	5.26	0.34
Felt 15	7.27	0.69
Felt 30	7.36	0.42
Felt 45	5.38	0.75
Felt 60	6.29	1.12

$$\varepsilon = (1 - \frac{\rho_{bulk}}{\rho_{sk}}) \cdot 100 \quad (3)$$

where ε is the void fraction (degree of voids) [%], ρ_{bulk} is the bulk density of the sample [kg·m^{-3}], and ρ_{sk} is the skeletal density of the sample [kg·m^{-3}].

The bulk density values of the nickel felt samples are reported in Table 4. The corresponding void fraction was calculated accordingly.

Table 4. Bulk density values of the nickel felt samples determined by analytical balance and caliper measurements.

	Bulk Density [g/cm^3]
Felt	1.694
Felt 7.5	1.668
Felt 15	1.631
Felt 30	1.707
Felt 45	1.247
Felt 60	1.898

The void fraction of the samples is calculated in the same way, and the resulting data are reported in a corresponding table (Table 5).

Table 5. Void fraction values obtained for the nickel felts, with the corresponding absolute standard deviations.

	Void Fraction [%]	Dev. Absolute Standard [%]
Felt	52.4	1.2
Felt 7.5	68.3	1.9
Felt 15	77.4	2.0
Felt 30	76.7	1.3
Felt 45	76.4	3.4
Felt 60	68.8	7.0

Pycnometric measurements were carried out to estimate the skeletal density of the nickel-based samples. The measured values show some dispersion, with an average value of approximately 6.3 g·cm^{-3}, which is lower than the intrinsic skeletal density of bulk metallic nickel (8.9 g·cm^{-3}). This discrepancy does not reflect a modification of the intrinsic density of nickel, but rather arises from the formation of microvoids within the electrodeposited layer and from the intrinsic limitations of water pycnometry when applied to highly porous and fibrous structures [17]. In such materials, incomplete liquid penetration into microvoids and tortuous pore networks leads to the determination of an

apparent skeletal density, which is therefore expected to be lower than the true skeletal density of massive nickel.

The high void fraction observed for all samples is therefore consistent with the intrinsic morphology of the nickel felt, which is characterized by an interconnected network of fibers and a large open porosity. Such structural features are desirable for MCFC electrode applications, as they promote effective gas transport and electrolyte retention. The dispersion observed in the calculated void fraction for nominally identical samples can be mainly ascribed to the intrinsic limitations of water pycnometry when applied to highly porous and fibrous materials. In particular, incomplete pore filling, air entrapment, and progressive liquid penetration within the open pore network may introduce variability in the measured values, affecting the repeatability of the technique and justifying the observed standard deviation.

3.3. Performance Test in Cell

The fabricated electrodes were evaluated in validated MCFC test stations to assess their performance under realistic operating conditions. A single nickel-plated cathode was chosen for cell testing, following preliminary experiments which demonstrated that the electrodeposition process significantly alters the nickel felt morphology.

The specific electrode selected for performance testing (30 min deposition at 1 A) possesses the same deposited mass as case (d) in Figure 1 (10 min at 3 A). This condition was prioritized because, as detailed in Table 5, lower current densities combined with longer deposition times yield a higher void fraction for a given mass. This resulting morphology optimizes porosity, facilitating efficient gas transport and superior electrolyte retention.

SEM analysis (Figure 4) revealed that the treated nickel felt exhibits an inter-fiber spacing of approximately 5–30 μm, which represents the effective pore size of the electrode. Although this range is slightly broader than the standard literature targets for MCFC cathodes (7–15 μm), it marks a substantial improvement over the pristine substrate (20–50 μm) where the spacing is considerably larger and further from the desired specifications. These morphological refinements render the nickel-plated felt far more suitable for electrochemical characterization than the untreated material, providing a representative electrode configuration with an open, interconnected porous structure.

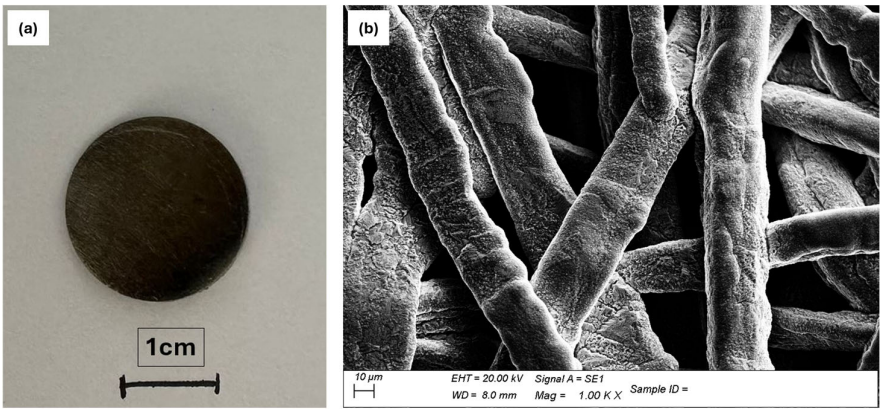

Figure 4. (**a**) Nickel felt electrode after electrodeposition (19 mm diameter); (**b**) SEM image of the nickel felt after nickel electrodeposition.

All other cell components consisted of well-established, reliable materials: the anode was Ni + 5 wt% Al (19 mm diameter); the electrolyte was a Li_2CO_3/K_2CO_3 eutectic mixture (62/38 mol%); and the matrix comprised two γ-$LiAlO_2$ sheets (25 mm diameter, 0.3 mm thickness) [18].

The choice of manufacturing circular-shaped electrodes presents both advantages and limitations, particularly when small-area cells are employed. In such configurations, edge effects may arise due to non-uniform current distributions and gas flows at the electrode boundaries, becoming more pronounced as the active area decreases and failing to represent the behavior of the central region of the cell [19]. Adopting a circular geometry, free of corners, helps mitigate these distortions and promotes a more uniform current distribution along the electrode perimeter. Regarding gas supply, the cathode is fed with a humidified mixture of air and CO_2, while the anode receives a humidified mixture of H_2 and CO_2. In Table 6 and in Table 7, the volumetric percentages of the gas streams supplied to the cathodic and anodic sides, respectively, are reported.

Table 6. Gas composition used for cathodic side.

Compounds	Composition [% *v*/*v*]
CO_2	28.8
O_2	14.4
H_2O	4.0
N_2	52.8

Table 7. Gas composition used for anodic side.

Compounds	Composition [% *v*/*v*]
CO_2	16.0
H_2O	20.0
H_2	64.0

Humidification plays a crucial role by limiting the formation of solid carbon deposits at high temperatures, thus suppressing carbon deposition via the Boudouard reaction, and, on the anode side, by promoting the water–gas shift reaction.

To evaluate the electrochemical performance of the fabricated electrode under MCFC operating conditions, three complementary characterization methods were employed: the current–voltage (I–V) curve, the corresponding power density curve, and electrochemical impedance spectroscopy (EIS). Each technique provides specific and complementary information on cell behavior and performance.

The I–V curve describes the evolution of the cell voltage as a function of the applied current density and represents a primary tool for assessing overall cell performance. From this curve, key parameters such as the open-circuit voltage (OCV), the operational voltage range, and the dominant loss mechanisms namely activation, ohmic, and concentration losses can be identified. The corresponding power density curve, obtained from the product of current density and cell voltage, provides direct insight into the maximum achievable power output and the optimal operating region of the cell. Both curves are reported in Figure 5 for the nickel felt electrode, with the I–V curve shown in blue and the power density curve shown in red.

Electrochemical impedance spectroscopy (EIS) was employed to gain deeper insight into the individual resistance contributions governing cell performance. By analyzing the impedance response over a wide frequency range, it is possible to separate ohmic resistance from charge-transfer and mass-transport-related processes occurring at the electrode and at the electrode-electrolyte interface. EIS therefore allows a more detailed interpretation of the polarization behavior observed in the I–V curves and helps identify performance-limiting phenomena (Figure 6).

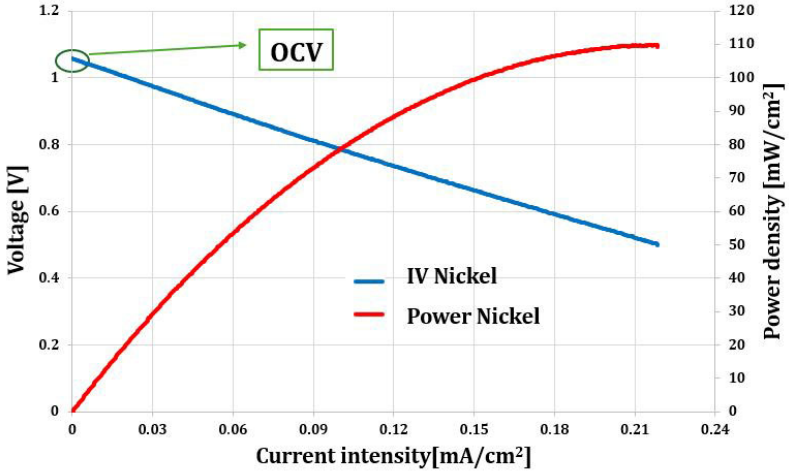

Figure 5. IV and power density curves of the tested nickel felt electrode. The IV curve is shown in blue, while the corresponding power density curve is shown in red.

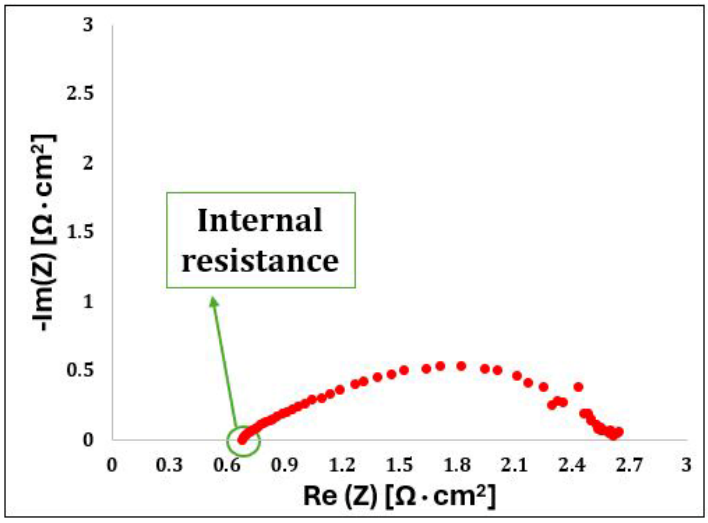

Figure 6. EIS curve of the nickel felt electrode, shown in red. The intercept of the curve with the *x*-axis provides the internal resistance of the electrode.

The internal (ohmic) resistance was obtained from the high-frequency intercept of the EIS Nyquist plot with the real axis, while the polarization resistance was determined from the difference between the low- and high-frequency intercepts of the impedance curve Table 8.

Table 8. Internal (ohmic) and polarization resistance values obtained from EIS analysis.

Internal Resistance [Ω·cm^2]	Polarization Resistance [Ω·cm^2]
0.6	2

The results obtained from the analysis of the I-V curve show good agreement with the experimental data reported in the literature for molten carbonate fuel cells. In particular, the measured open-circuit voltage (OCV) is 1.05 V, which is in excellent accordance with typical values reported for similar systems [19]. Likewise, the maximum power output of the cell reaches approximately 110 W, compared to a reference value of 125 W found in the literature, indicating overall performance consistent with the state of the art [20]. Furthermore, electrochemical impedance spectroscopy analysis allowed the estimation of an internal resistance of 0.60 Ω·cm^2, a value very close to the 0.55 Ω·cm^2 reported in

previous studies, further confirming the reliability and validity of the experimental results obtained [21,22].

4. Conclusions

This study demonstrates that galvanostatic electrodeposition on nickel felt substrates is an effective and reproducible manufacturing route for producing porous nickel cathodes suitable for molten carbonate fuel cell applications. By controlling the applied current and deposition time, the deposited mass was shown to scale linearly with the current–time product, in good agreement with Faraday's law and with a coefficient of variation below 10%, confirming the robustness and predictability of the process.

SEM analysis revealed a progressive and uniform growth of the nickel coating with increasing deposition time, resulting in improved coating continuity while preserving the intrinsic fibrous morphology of the felt substrate. Importantly, the open and interconnected pore network was maintained even at higher deposited masses, a key requirement to ensure effective gas diffusion and electrolyte retention in MCFC cathodes.

High-temperature oxidation tests conducted at 700 °C under oxidizing atmosphere showed a parabolic oxidation behavior characteristic of diffusion-controlled kinetics. The extracted parabolic rate constant, on the order of 10^{-10} $g^2 \cdot cm^{-4} \cdot s^{-1}$, is consistent with literature values reported for nickel at comparable temperatures, confirming the thermal and chemical stability of the electrodeposited nickel structures under conditions representative of MCFC operation.

Density and porosity characterization highlighted void fractions in the range of approximately 68%–77%, in line with the felt-based architecture and compatible with cathodic operation. At the same time, the dispersion observed in skeletal density and void fraction values emphasized the intrinsic limitations of conventional water pycnometry when applied to highly porous and fibrous materials, indicating the need for complementary and pore-size-resolved characterization techniques.

Single-cell electrochemical testing demonstrated the functional effectiveness of the electrodeposited nickel felt when operated as a cathode under MCFC conditions. The measured open-circuit voltage (~1.05 V), maximum power output (~110 mW/cm^2), and internal resistance (~0.60 $\Omega \cdot cm^2$) showed good agreement with reference data for conventional MCFC electrodes, indicating that the electrodeposition-based approach can achieve competitive performance at the laboratory scale.

Future work will focus on further optimizing the electrodeposition parameters to tailor the pore size distribution and overall porosity toward the target values reported in the literature for MCFC cathodes.

Author Contributions: Conceptualization, M.P. and B.B.; Methodology, M.P. and B.B.; Formal analysis, R.S. and B.B.; Investigation, M.P., D.B. and R.S.; Resources, M.P., R.S. and B.B.; Data curation, D.B. and B.B.; Writing—original draft, M.P.; Writing—review & editing, D.B., R.S. and B.B.; Visualization, M.P., D.B., R.S. and B.B.; Supervision, M.P., D.B., R.S. and B.B.; Project administration, R.S., D.B. and B.B. All authors have read and agreed to the published version of the manuscript.

Funding: This research was partially funded by the project CALIPSO—Celle a combustibile innovative ad alta potenza in sistemi stazionari e di mobilità. PNRR—Prog. n. RSH2A_000021—CUP: F57G25000200006.

Institutional Review Board Statement: Not applicable.

Informed Consent Statement: Not applicable.

Data Availability Statement: The original contributions presented in this study are included in the article. Further inquiries can be directed to the corresponding author.

Acknowledgments: The authors gratefully acknowledge Juan Pedro Pérez Trujillo and Carina Lagergren of Applied Electrochemistry, Department of Chemical Engineering, KTH Royal Institute of Technology for the collaboration in the button MCFC experimental test.

Conflicts of Interest: The authors declare no conflict of interest.

References

1. O'Hayre, R.; Cha, S.-W.; Colella, W.; Prinz, F.B. *Fuel Cell Fundamentals*; Wiley: Hoboken, NJ, USA, USA, 2016.
2. Sørensen, B. *Hydrogen and Fuel Cells: Emerging Technologies and Applications*; Elsevier: Amsterdam, The Netherlands, 2012.
3. Sheikh, A.A.; Bianchi, F.R.; Bove, D.; Bosio, B. A review on MCFC matrix: State-of-the-art, degradation mechanisms and technological improvements. *Heliyon* **2024**, *10*, e25847. [CrossRef] [PubMed]
4. Risso, R.; Bove, D.; Bosio, B. Comparative Analysis of Different On-Board CCS Molten Carbonate Fuel Cell Solutions for IMO Compliance. *Energies* **2023**, *16*, 6748. [CrossRef]
5. Spinelli, M.; Romano, M.C.; Consonni, S.; Campanari, S.; Marchi, M.; Cinti, G. Application of Molten Carbonate Fuel Cells in Cement Plants for CO_2 Capture and Clean Power Generation. *Energy Procedia* **2014**, *63*, 6517–6526. [CrossRef]
6. Austen, Y.; Bove, D.; Cannizzaro, F.; Palmisani, E.; Bosio, B. Exploring the Potential of Molten Carbonate Fuel Cells for CO_2 Capture and Concentration: A Feasibility Analysis in the Steel Industry. *Energy Fuels* **2025**, *39*, 23703–23714. [CrossRef] [PubMed]
7. Hall, J.L. *Fuel Cell Handbook*, 7th ed.; National Energy Technology Laboratory: Pittsburgh, PA, USA, 2002.
8. Riporti Galvanici Group. NICHELATURA. Available online: https://www.riportigalvanici.it/lavorazioni-galvaniche/nichelatura/ (accessed on 25 December 2025).
9. Tambe, C.E.; Green, T.A.; Roy, S. The multifaceted role of boric acid in nickel electrodeposition and electroforming. *J. Electrochem. Soc.* **2024**, *171*, 102503. [CrossRef]
10. Seveso, P. *Isprambiente-Descrizione dei Trattamenti Galvanici*; Portale Seveso: Rome, Italy, 2024.
11. Bard, A.J. *Electrochemical Methods: Fundamentals and Applications*; Wiley: Hoboken, NJ, USA, 2001.
12. Schlesinger, M.; Paunovic, M. *Modern Electroplating*; Wiley: Hoboken, NJ, USA, 2010.
13. Box, E.P.B.; Hunter, J.S.; Hunter, W.G. *Statistics for Experimenters*; Wiley: Hoboken, NJ, USA, 2005.
14. Progar, D.J.; Lewis, B.W. A Study of Oxidation Kinetics of Nickel Metal in Flowing Air and Oxygen-Nitrogen Mixtures. No. December; 1964; pp. 1–57. Available online: https://ntrs.nasa.gov/api/citations/19650002476/downloads/19650002476.pdf (accessed on 25 December 2025).
15. Rose, I.; Whittington, C. *Nickel Plating Handbook*; Nickel Institute: Toronto, Canada, 2013; pp. 263–292.
16. Kubaschewski, O.; Hopkins, B.E. *The Oxidation of Metals*; Butterworths: London, UK, 1962.
17. Dharmaraj, K.; Lauermann, R.H.; Bagacki, R.; Xi, F.; Kemppainen, E.; Schlatmann, R.; Calnan, S. Electrodeposited Porous Nickel–Copper as a Non-Noble Metal Catalyst for Urea-Assisted Anion Exchange Membrane Electrolysis for Hydrogen Production. *ACS Sustain. Chem. Eng.* **2024**, *12*, 9908–9921. [CrossRef]
18. Choi, H.J.; Lee, J.J.; Hyun, S.H.; Lim, H.C. Fabrication and performance evaluation of electrolyte-combined α-$LiAlO_2$ matrices for molten carbonate fuel cells. *Int. J. Hydrogen Energy* **2011**, *36*, 11048–11055. [CrossRef]
19. Hall, J.L. Fuel Cell Handbook. *Phytochemistry* **1987**, *26*, 1235–1236. [CrossRef]
20. Choi, H.-J.; Lee, J.-J.; Hyun, S.-H.; Lim, H.-C. Performance and Durability of the Molten Carbonate Electrolysis Cell and the Reversible Molten Carbonate Fuel Cell. *Int. J. Hydrogen Energy* **2011**, *36*, 11048–11055. [CrossRef]
21. Leng, Y. *Materials Characterization: Introduction to Microscopic and Spectroscopic Methods*; Wiley: Hoboken, NJ, USA, 2008.
22. Hashibon, A.; Raz, S.; Riess, I. Preferred position for the reference electrode in solid state electrochemistry. *Solid State Ion.* **2002**, *149*, 167–176. [CrossRef]